Stabilization regimes and pollutant emissions from a dual fuel CH4/H2 and dual swirl low NOx burner

Sylvain Marragou, Hervé Magnes, Thierry Poinsot, Laurent Selle, Thierry Schuller

Stabilisation regimes and pollutant emissions from a dual fuel CH4/H2 and dual swirl low NOx burner

S. Marragou[a,*], H. Magnes[a], T. Poinsot[a], L. Selle[a], T. Schuller[a]

[a]*Institut de Mécanique des Fluides de Toulouse, IMFT, Université de Toulouse, CNRS, Toulouse, France*

Abstract

Burning hydrogen in gas turbines is a relevant technological solution to decarbonise power production and propulsion systems. However, ensuring low NOx emission and preventing flashback can be challenging with hydrogen. Stabilisation regimes and pollutant emissions from partially premixed CH4/H2/air flames above a coaxial Dual Fuel Dual Swirl injector are investigated in a laboratory-scale combustor at atmospheric conditions for increasing hydrogen contents. The injector consists of an external annular swirler providing premixed methane/air and a central channel fed with pure hydrogen. This burner virtually removes the risk of flashback due to the late injection of hydrogen. Flame stabilisation regimes, CO and NOx emissions are analysed for different configurations of the injector and operating points. The effect of swirling the hydrogen stream is investigated together with the influence of the hydrogen injector recess, i.e. its nozzle position with respect to the backplane of the combustion chamber. It is shown that swirling the central hydrogen stream favours aerodynamically stabilised flames resulting in a low thermal stress on the injector and limited NOx emissions. The study also highlights that a small recess of the central hydrogen injector widely extends the operability range of the burner with aerodynamically stabilised flames. With a sufficient inner swirl and a small recess, flames detach from the injector rim when the hydrogen bulk velocity is large enough. In this configuration, it is found that NOx emissions remain low even for operation with pure hydrogen. Moreover, NOx emissions decrease when increasing the thermal power for a fixed equivalence ratio.

Keywords: `Hydrogen combustion, Swirled burner, Coaxial injector, Lifted flame, Gas turbine`

1. Introduction

In order to achieve the necessary reduction of greenhouse-gas emissions and lower NOx emission levels, lean premixed combustion of hydrogen-enriched fuel blends is seen as a promising path for the gas turbine industry [1]. Many gas turbines are already fuel flexible and can burn hydrocarbon and hydrogen fuel blends in variable proportions [2, 3].

The higher adiabatic temperature of hydrogen flames compared to hydrocarbon fuelled flames at the same equivalence ratio and their propensity to burn in diffusion regime usually leads to higher NOx emissions and may also cause mechanical damage to the engines [1, 4, 5]. Risks of flashback, undesired autoignition and dynamic issues rapidly increase with the hydrogen content in fuel blend due to its increased reactivity [5, 6, 7]. To overcome these issues, one possibility is to inject hydrogen as late as possible in the combustion chamber. The challenge is then to mix hydrogen and air sufficiently fast before combustion. This has led to the development of micromixing technologies [8] to avoid the formation of high-temperature stoichiometric reaction layers at the hydrogen injector outlet, which are responsible for high NOx emissions levels (see for examples [9, 10]) and high thermal stress. Micromixing injection devices are disruptive technologies that require a completely new design of the combustor with respect to conventional gas turbines operating with swirl burners [11].

An alternative is presented in this study, in which hydrogen is injected in a conventional swirl burner. The system allows partial premixing of hydrogen with the oxidiser before combustion to avoid the formation of diffusion reaction layers anchored to the fuel nozzle that penalise NOx emissions.

Swirling the air flow is the standard way of stabilising flames in gas turbines away from the solid components of the burner by a central recirculation zone (CRZ) [12]. There are many ways to inject the fuel in a swirling air channel to favour its mixing with air (see for examples [8, 13, 14]). One of the simplest is to inject the fuel as a jet through a central lance in a co-axial injector in which the air stream is swirled. Analysis of the flow structure above co-axial injectors with swirl vanes reveals that above a critical swirl level in the central injector and in the annular channel, and

*Corresponding author: sylvain.marragou@toulouse-inp.fr

with an adapted impulsion ratio between the two streams, a stable CRZ can be obtained above the injector in cold [15] as well as hot-flow conditions [16, 17]. This robust rotating structure enables aerodynamic stabilisation of the combustion zone above the coaxial injector outlet. However, the momentum of the fuel jet pushes the CRZ further downstream and may eventually destroy the CRZ for too high fuel jet injection velocities with respect to the swirl level impregnated to the air flow [7, 15, 16, 17].

A second possibility is to add a swirl vane in the fuel injection lance. Adding swirl to a central lance was found to improve mixing with a co-axial non swirling annular air flow in the simulations carried out in [18]. The authors also found that mixing improves for injection of light gases in the central lance as hydrogen. In an analysis of flame stabilisation above coaxial injectors in which both the annular air and central fuel channels are swirled, Yuasa [19] observed that swirling the fuel jet helps lifting methane flames, but hydrogen flames remain anchored to the hydrogen injector rim even for sonic hydrogen injection conditions. It has recently been shown that a coaxial burner with a strong swirl level impregnated to a central methane stream enables to lift the flame above the burner nozzle even when the annular air channel is enriched with oxygen [20, 21]. Due to the strong reactivity of oxygen, a non-swirling fuel jet produces a diffusion flame anchored on the fuel nozzle rim independently of the swirl level conferred to the oxidiser stream.

This injection strategy with swirl imparted to the central fuel stream is here further investigated for hydrogen injection in a swirling annular flow and different geometric configurations of a co-axial injector. In particular, the combined role of internal swirl level and hydrogen injector recess is examined. Pollutant emissions should be assessed for this fuel and air injection system. Flame stabilisation and pollutants are addressed in the present work with a Dual Fuel Dual Swirl (DFDS) burner developed at IMFT laboratory.

The DFDS burner described in section 2 is used to analyse flame stabilisation from methane air mixtures flowing through a swirled annular channel with a pure hydrogen swirling flow exhausting from a central lance when the power from methane combustion is progressively replaced by hydrogen. A parametric analysis is first carried out in section 3 to identify the geometric parameters and the flow variables controlling flame stabilisation leading to anchored or aerodynamically stabilised flames for a given burner geometry. More specifically, the impact of the hydrogen bulk

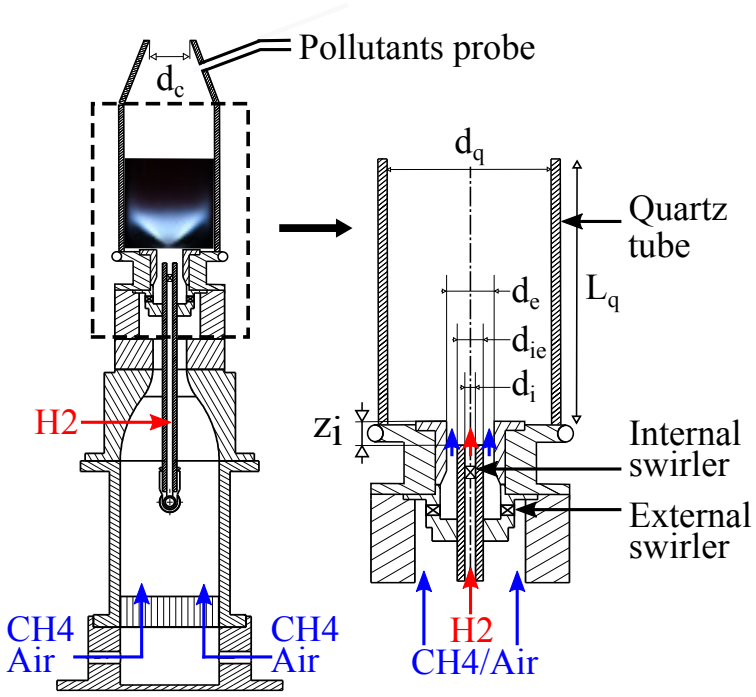

Fig. 1. Experimental setup.

injection velocity, equivalence ratio, hydrogen content, internal swirl level provided to the hydrogen flow and the position of the fuel lance with respect to the burner nozzle outlet are examined. Five typical cases are then considered in section 4 for which a more detailed analysis of the flame topology is carried out by examining OH^* emission intensity distributions. Finally, CO and NOx emissions are measured and compared to operation for perfectly premixed methane/air injection conditions in section 5.

2. Experimental setup

2.1. MIRADAS DFDS

The burner used for this study is an evolution of the MIRADAS setup [22, 23]. A schematic of this version called MIRADAS DFDS for Dual Fuel Dual Swirl is represented in Fig. 1. This injection system has recently been patented [24]. Methane, hydrogen and air flow rates injected in the burner are monitored by three mass flow regulators Brooks SLA 585x series. Premixed

methane and air are injected at the bottom of a cylindrical plenum of 65 mm diameter and 100 mm length. The plenum is fitted with a perforated plate at the bottom and three honeycomb structures in order to homogenise the flow and break down turbulent fluctuations. The mixture then passes through a convergent of 75 mm length, contracting the flow through a 22 mm diameter nozzle followed by a radial swirl vane with $n = 8$ cylindrical channels of $d_h = 4$ mm diameter making an angle $\alpha_e = 42^\circ$ with the radial direction.

This device generates a flow characterised by a swirl number $S_e = 0.67$ computed by assuming a uniform profile for the axial velocity and a solid body rotation for the azimuthal velocity in the annular channel of internal diameter $d_{ie} = 10$ mm and external diameter $d_e = 18$ mm.

Hydrogen is injected through a central lance of internal diameter $d_i = 6$ mm and external diameter $d_{ie} = 10$ mm aligned on the axis of the annular methane/air injector. The outlet of the central hydrogen lance has a variable recess $z_i = 0$ or $z_i = 4$ mm with respect to the annular injector outlet. Two different axial vanes can be placed inside the hydrogen fuel lance, 10 mm upstream the outlet section, with different tail angles $\alpha_i = 0^\circ$ and 61° respectively corresponding to internal swirl numbers $S_i = 0.0$ and $S_i = 0.9$ computed via:

$$S_i = \frac{1}{2}\tan(\alpha_i) \tag{1}$$

With these possible variations in the DFDS burner, four cases are considered. First, the baseline configuration, denoted B, is the case without internal swirl $S_i = 0$ and no recess $z_i = 0$. The configuration with swirl $S_i \neq 0$ in the central lance and without recess $z_i = 0$ is denoted S. Adding the $z_i = 4$ mm recess to these cases results in two additional configurations, denoted respectively BR and SR depending on whether the central lance is equipped with a swirl vane.

The methane/air and hydrogen jets exhausting from the co-axial injector expand in a cylindrical combustion chamber made of quartz. The quartz tube has an internal diameter $d_q = 64$ mm and a length $L_q = 100$ mm. At the top of the quartz tube, a stainless steel cone is placed to maintain the flow recirculation regions inside the combustion chamber and prevent dilution of burned gases by ambient air, which would skew pollutant emission measurements. The outlet diameter of this nozzle is $d_c = 48$ mm corresponding to a contraction ratio of 0.57 with respect to the combustion chamber cross-section area.

2.2. Diagnostics

A Nikon D7500 with a lens Nikon AF-S VR Micro-Nikkor 105mm f/2.8G IF-ED is used for direct flame visualization. Flame images are also taken in the UV band with a Princeton PI-MAX4 ICCD camera equipped with a Nikon Rayfact UV-105 Multispectral lens, 105 mm f/4.5 and a bandpass filter centered on $\lambda = 310 \pm 10$ nm Asahi XHQA310. The selected wavelength band enables recording the chemiluminescence of the OH^* radical used as a tracer of heat release rate [25]. Pollutant emissions are measured with an ECOM J2KN Pro flue gas analyzer featuring a confidence interval of ±5% of the measured value for NO and NO_2 concentrations and ±3% for CO in the dried sampled flue gases. Resolution is 0.1 ppm for NO and NO_2 concentrations and 1 ppm for CO. Only NOx measurements are presented in this study without differentiating NO from NO_2.

2.3. Experimental protocol

The experimental bench is monitored by a Labview program controlling the flow regulators. The input values are a reference bulk velocity u_{e0} of the methane/air mixture in the annular channel, a reference global equivalence ratio ϕ_0 of the methane/air mixture and the fraction PHx with $x = 0$ to 100% of thermal power from hydrogen combustion with respect the total thermal power P_{th} released by the flame. The fully premixed methane case is denoted Ref. All experiments are made with fluids injected at ambiant temperature and in a combustion chamber operating at atmospheric pressure.

Experiments are carried out by setting the reference bulk velocity u_{e0} and reference equivalence ratio ϕ_0 for the methane/air mixture injected through the annular channel of the DFDS burner. Values for u_{e0} are deduced from methane and air massflow regulators for an annular flow injected at ambient conditions in the annular channel of internal diameter d_{ie} and external diameter d_e. When hydrogen is injected, the total thermal power P_{th} and air mass flowrate $\dot{m}_a$ are kept constant. Methane is removed from the external channel and replaced by hydrogen injected through the central tube to get the desired fraction of power PHx originating from hydrogen. As a consequence, the bulk velocity u_e in the annular channel and the global equivalence ratio ϕ at which the DFDS burner operates slightly differ from the reference values u_{e0} and ϕ_0 set for methane/air

operation when increasing the hydrogen content PHx.

The global equivalence ratio is defined here as:

$$\phi = s\frac{\dot{m}_{CH4} + \dot{m}_{H2}}{\dot{m}_a}, \tag{2}$$

where $\dot{m}_{CH4}$, $\dot{m}_{H2}$, $\dot{m}_a$ denote the mass flowrates of methane, hydrogen and air. The stoichiometric ratio s is:

$$s = \frac{(2 - 1.5X_{H2})\,(W_{O2} + 3.76W_{N_2})}{X_{CH4}W_{CH4} + X_{H2}W_{H2}} \tag{3}$$

where X_{CH4} and X_{H2} are the molar fractions of methane and hydrogen in CH_4/H_2 fuel blend and W_{O2}, W_{N2}, W_{CH4} and W_{H2} denote the molar masses of oxygen, nitrogen, methane and hydrogen.

All flow parameters, the hydrogen injection velocity u_i in the internal channel, the equivalence ratio ϕ_e of the CH4/air mixture in the external channel, the global equivalence ratio ϕ and the momentum ratio $J = \rho_e u_e^2/\rho_i u_i^2$ between the external and internal flow streams are reported in Tab. 1 for injection at ambient conditions $T_a = 293$ K and $p_a = 1$ atm.

With variations in geometry, bulk velocity, equivalence ratio and power fraction from hydrogen, there are 44 flames presented in this study. A compact notation is proposed to facilitate their description: $Geo - u_{e0} - \phi_0 - PHx$, where Geo can be B, BR, S or SR, u_{e0} can take the values 12, 24 or 30 m/s and ϕ_0 is 0.55, 0.65 or 0.75. These configurations are summarised in Tab. 2.

Tab. 1. Operating conditions

u_{e0} [m/s]	ϕ_0	P_{th} [kW]		Ref	PH20	PH40	PH60	PH80	PH100
12	0.75	5.2	u_e [m/s]	12.0	11.9	11.7	11.5	11.3	11.2
			u_i [m/s]	0.0	3.6	7.3	11.0	14.5	18.2
			ϕ	0.75	0.72	0.69	0.67	0.64	0.62
			ϕ_e	0.75	0.60	0.45	0.30	0.15	0.0
			J	∞	151	37	16	9	5
12	0.65	4.5	u_e [m/s]	12.0	11.9	11.7	11.6	11.4	11.3
			u_i [m/s]	0.0	3.2	6.4	9.5	12.7	15.9
			ϕ	0.65	0.62	0.60	0.58	0.56	0.54
			ϕ_e	0.65	0.52	0.39	0.26	0.13	0.0
			J	∞	198	49	21	12	7
12	0.55	3.9	u_e [m/s]	12.0	11.9	11.8	11.6	11.5	11.4
			u_i [m/s]	0.0	2.7	5.4	8.1	10.9	13.6
			ϕ	0.55	0.53	0.51	0.49	0.47	0.45
			ϕ_e	0.55	0.44	0.33	0.22	0.11	0.0
			J	∞	274	67	29	16	10
24	0.75	10.3	u_e [m/s]	24.0	23.8	23.4	23.0	22.7	22.3
			u_i [m/s]	0.0	7.3	14.5	21.8	29.9	36.3
			ϕ	0.75	0.72	0.69	0.67	0.64	0.62
			ϕ_e	0.75	0.60	0.45	0.30	0.15	0.0
			J	∞	151	37	16	9	5
24	0.65	9.0	u_e [m/s]	24.0	23.8	23.5	23.2	22.8	22.5
			u_i [m/s]	0.0	6.4	12.7	19.1	25.4	31.8
			ϕ	0.65	0.62	0.60	0.58	0.56	0.54
			ϕ_e	0.65	0.52	0.39	0.26	0.13	0.0
			J	∞	198	49	21	12	7
24	0.55	7.7	u_e [m/s]	24.0	23.8	23.5	23.3	23.0	22.8
			u_i [m/s]	0.0	5.4	10.9	16.3	21.7	27.2
			ϕ	0.55	0.53	0.51	0.49	0.47	0.45
			ϕ_e	0.55	0.44	0.33	0.22	0.11	0.0
			J	∞	274	67	29	16	10
30	0.75	12.9	u_e [m/s]	30.0	29.7	29.2	28.8	28.4	27.9
			u_i [m/s]	0.0	9.1	18	27.2	36.3	45.4
			ϕ	0.75	0.72	0.69	0.67	0.64	0.62
			ϕ_e	0.75	0.60	0.45	0.30	0.15	0.0
			J	∞	151	37	16	9	5
30	0.65	11.3	u_e [m/s]	30.0	29.7	29.3	29.0	28.6	28.2
			u_i [m/s]	0.0	7.9	15.9	23.8	31.8	39.7
			ϕ	0.65	0.62	0.60	0.58	0.56	0.54
			ϕ_e	0.65	0.52	0.39	0.26	0.13	0.0
			J	∞	198	49	21	12	7
30	0.55	9.7	u_e [m/s]	30.0	29.8	29.5	29.1	28.8	28.5
			u_i [m/s]	0.0	6.8	13.6	20.4	27.2	34.0
			ϕ	0.55	0.53	0.51	0.49	0.47	0.45
			ϕ_e	0.55	0.44	0.33	0.22	0.11	0.0
			J	∞	274	67	29	16	10

Tab. 2. Summary of all possible configurations and operating points with the nomenclature $Geo - u_{e0} - \phi_0 - PHx$.

Geo	u_{e0} [m/s]	ϕ_0	PHx
B : $S_i = 0.0$, $z_i = 0$ mm	12	0.55	Ref
BR: $S_i = 0.0$, $z_i = 4$ mm	24	0.65	PH20
S : $S_i = 0.9$, $z_i = 0$ mm	30	0.75	PH40
SR: $S_i = 0.9$, $z_i = 4$ mm			PH60
			PH80
			PH100

3. Parametric analysis of flame stabilisation

Flame stabilisation is first studied for a fixed external swirl level, $S_e = 0.67$, and different geometrical configurations of the burner to assess the effects of the inner swirl level S_i and injector recess z_i when the reference bulk velocity u_{e0}, reference global equivalence ratio ϕ_0 and thermal power PHx from hydrogen are varied, while keeping the total thermal power P_{th} constant. In addition to the Ref case, five levels of hydrogen injection are studied, $PH20$, $PH40$, $PH60$, $PH80$ and $PH100$. The case $PH100$ corresponds to pure hydrogen combustion.

Pressure drops in both injection channels are indicated in Tab. 3 for three operating conditions. In the central injection channel, the pressure drop Δp_i corresponds to the difference between the static pressure below the axial swirl vane in the 6 mm fuel channel and ambiant pressure. In the external channel, Δp_e corresponds to the difference between the static pressure measured below the radial swirl vane and ambiant pressure. In both channels, the pressure drop increases linearly with the dynamic pressure $1/2\rho u^2$. In the external channel, it reaches 5.3% of ambient pressure for the highest thermal power $P_{th} = 12.9$ kW for $SR - 30 - 0.75 - PH100$. The radial swirling vane used in this study was not optimized to minimize the pressure drop so that it is difficult to make any interpretation regarding some optimal configuration with respect to pressure drop. For the same case $SR - 30 - 0.75 - PH100$, despite the highest hydrogen injection velocity than the air

Tab. 3. Pressure drops Δp_e in the annular channel and Δp_i in the central channel for 3 operating conditions. Values are averaged over 10 s measurements. The dynamic pressures based on the bulk flow velocities are also indicated.

$[Pa]$	Δp_e	$1/2\rho_e u_e^2$	Δp_i	$1/2\rho_i u_i^2$
$SR-12-0.75-PH100$	899	74	492	13
$SR-24-0.75-PH100$	3504	293	1603	54
$SR-30-0.75-PH100$	5287	458	2397	84

velocity (see Tab. 1), the pressure drop in the hydrogen channel is limited to only 2.4% of ambient pressure due to the very low hydrogen density.

The flame can take three different topologies illustrated in Fig. 2. The first archetype shown in Fig. 2a corresponds to the fully premixed methane/air Ref case that is always anchored on the injector lip for all flow and geometrical configurations of the burner explored in this study. The three other archetypes in Figs. 2b, 2c and 2d correspond to partially premixed injection conditions in which a fraction of the methane mass-flow rate is removed from the external channel and replaced by hydrogen injected through the central fuel lance. Figures 2b and 2c encompasse partially premixed flames slightly protruding inside the external annular injector along the central hydrogen lance. These flames are designated as anchored on the hydrogen injector rim. The flame archetype in Fig. 2b is stabilised on the hydrogen nozzle rim by a reaction layer between the central pilot hydrogen jet and the annular methane/air jet. The reaction layer in the center is stabilised at the top of a weak central recirculation zone (CRZ). This archetype is only observed for non-swirling hydrogen jets. The flame in Fig. 2c features the same reaction layer anchoring the flame on the hydrogen nozzle. The difference with Fig. 2b is the reaction layer in the center of the flow, which is now stabilised close to the apex of the CRZ. This archetype is observed for swirled hydrogen jets featuring a strong CRZ. For the last flame archetype shown in Fig. 2d, the reaction layer in the shear layer between the central hydrogen jet and the annular jet is detached from the hydrogen nozzle and only persists a partially premixed flame in the center of the flow, which is aerodynamically stabilised above the coaxial injector at a small lift off height above the hydrogen nozzle. This pattern is observed for highly swirled hydrogen jets with a high hydrogen injection velocity.

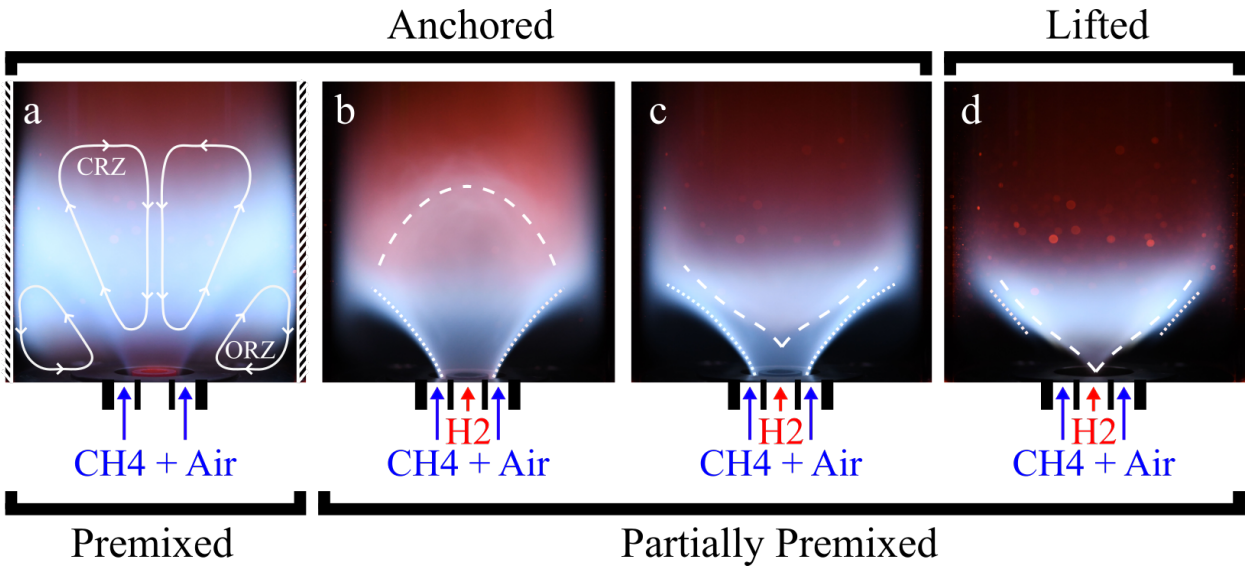

Fig. 2. Flame archetypes stabilised on the DFDS burner.(a) Premixed CH_4/air swirling flame with approximative locations of the Central Recirculation Zone (CRZ) and Outer Recirculation Zone (ORZ). The location of the sidewalls is also indicated. (b) Attached flame with non-swirling central hydrogen jet. (c) Attached flame with a swirling central hydrogen jet. (d) Lifted flame with a swirling central hydrogen jet. Dashed lines: shear layer stabilised flame. Dotted lines: central reaction layer.

3.1. Effect of inner swirl and recess

Consider first a configuration in which the internal hydrogen lance is flush mounted with the external annular channel outlet, i.e. $z_i = 0$ mm. The external CH_4/air stream is swirled $S_e = 0.67$. The internal channel is equipped with an axial swirl vane with a trailing edge angle $\alpha_i = 0$ resulting in a non-swirling hydrogen stream corresponding to case *B*. This fake internal swirl vane produces a pressure drop in the hydrogen channel flow and creates a wake flow downstream the swirler blades. Figure 3 shows the evolution of the flame shape for case $B-24-0.75-PHx$ where PHx is varied from Ref to PH100. Table 1 indicates that the bulk velocity u_e barely changes when methane is removed from the external channel, but the global equivalence ratio drops from $\phi = 0.75$ for methane/air Ref operation to $\phi = 0.62$ for hydrogen/air PH100 operation. The momentum ratio J, which is an important parameter controlling flame lift-off above co-axial injectors [17, 20] decreases as the fraction of H_2 increases.

For this baseline configuration obtained for $u_{e0} = 24$ m/s and $\phi_0 = 0.75$, Fig. 3 shows that all

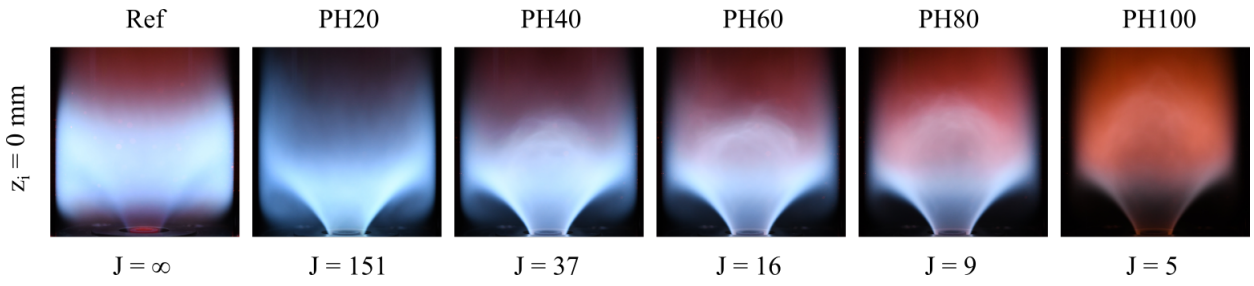

Fig. 3. Effect of the central hydrogen injection on flame stabilisation for $B-24-0.75-PHx$. Natural flame emission in the visible spectrum.

flames are anchored to the central fuel injector and take a V-shape as in Figs. 2a and 2b. The flame topology for cases Ref and PH20 in Fig. 3 corresponds to the flame archetype shown in Fig. 2a for low hydrogen injection velocities. For higher hydrogen injection velocities, the CRZ for cases PHX with $X \geq 40$ is destabilized by the high momentum of the central hydrogen jet and the flame takes the archetype shown in Fig. 2b. Varying the bulk velocity u_{e0} in the external annular channel or the equivalence ratio ϕ_0 does not change the stabilisation mode and yield similar results despite large variations of the momentum ratio J. For the baseline configuration B of the burner, i.e. no internal swirl and no recess of the hydrogen lance, flames are always anchored to the hydrogen rim independently of the range of momentum ratio J that was covered $1 \leq J \leq \infty$.

Differences between flames in Fig. 3 are only observed close to the combustion chamber sidewalls and at the top of the flame. The premixed methane/air Ref case on the left features reaction layers stabilised in the outer recirculation zone as in Fig. 2a close to the quartz wall that progressively disappear when the hydrogen content increases. As the hydrogen content increases, the velocity of the jet pushes the central reaction zone downstream and a halo forms at the top of the flame. For pure hydrogen injection PH100, the hydrogen injection velocity $u_i = 36.3$ m/s exceeds the bulk velocity $u_e = 22.3$ m/s in the annular channel leading to a drop in the momentum ratio to $J = 5$. Without internal swirl vane $S_i = 0$, the high penetration of the central fuel jet destabilises the CRZ when the momentum ratio J drops [15, 17, 26]. As a consequence, destabilization of the CRZ increases with the power originating from hydrogen. Similar results are obtained for the baseline configuration of the burner with recess denoted BR (no internal swirl, with recess). The

corresponding flame images are provided as supplemental material.

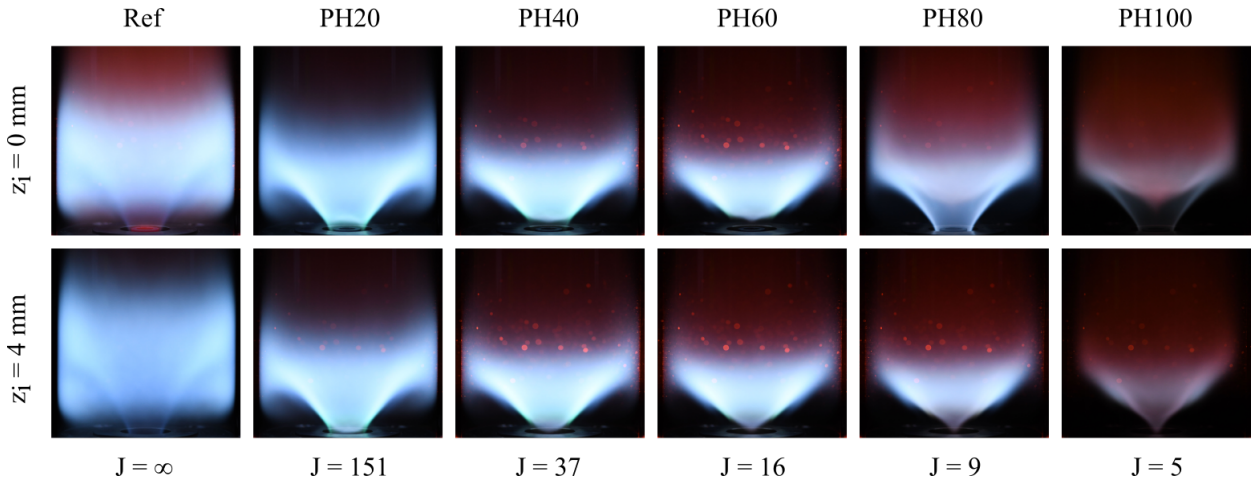

Fig. 4. Effect of inner swirl (top) and injector recess (bottom) on flame stabilisation respectively for $S-24-0.75-PHx$ and $SR-24-0.75-PHx$.Natural flame emission in the visible spectrum.

Following [19, 20, 21], the impact of swirling the fuel in the central lance is now investigated for configuration S of the burner with an internal swirling vane $S_i \neq 0$ but no recess $z_i = 0$ of the hydrogen lance. The top row in Fig. 4 shows the flame topologies for the cases $S-24-0.75-PHx$. Without flow in the central tube, the Ref case is identical but comparing cases B in Fig. 3 and cases S in Fig. 4, the PH20 cases are also similar. These two flames correspond again to the flame archetypes shown in Fig. 2a. However, as the hydrogen content is further increased, topologies become quite different. First, for PH40 and PH60, the halo of luminosity at the top of the flame observed without internal swirl in Fig. 3 has completely disappeared in Fig. 4. For PH40, the flame is lifted above the burner, but one still distinguishes a weak blue/green luminosity close to the central injector lip. Looking at instantaneous snapshots reveals that this pale brightness is associated to a reaction layer that intermittently attaches to the central injector lip, as also observed in [19] for methane and hydrogen flames.

Increasing further the hydrogen content to reach PH60, the flame becomes fully aerodynamically stabilised above the coaxial injector and more compact, corresponding to the flame archetype shown in Fig. 2d. This shape is attributed to the strong CRZ that protrudes along the burner axis leading to high radial velocities and high strain rates at the lips of the central fuel lance [21].

The radial deflection of the hydrogen flow leads to fast mixing between the methane/air mixture exhausting from the annular channel and the swirled hydrogen jet above the fuel lance [16, 18].

By further increasing the hydrogen content to PH80 and PH100, the flame reattaches to the central injector rim and corresponds to the flame archetype shown in Fig. 2c. In these cases, the impulsion ratio J is lower than the density ratio between the two streams, indicating that the bulk injection velocity u_i of hydrogen in the central lance is greater than the bulk velocity u_e of the external annular stream at the co-axial injector outlet. A too strong hydrogen velocity pushes the CRZ further downstream due again to the drop of the momentum ratio J [15, 16, 17]. Flame reattachment at small values of the momentum ratio J was also identified in [21] for methane oxy-flames. These experiments without recess confirm that high hydrogen injection velocities lead to flame reattachment to the central injector.

The main conclusion is that a high internal swirl level is necessary to lift the flame, but is not sufficient to maintain this stabilisation regime for flames with a high hydrogen content, and more specifically for pure hydrogen injection when the impulsion ratio J between the two streams is low. This observation was found to be valid for all cases explored in this study and also valid over a wide range of other operating conditions, which are not reported here for conciseness. In order to prevent flame reattachment, an additional geometrical modification is investigated by changing the injector recess, i.e. the axial position z_i of the central hydrogen lance outlet with respect to the annular channel outlet of the coaxial DFDS burner.

Figure 4 at the bottom shows the shapes of the flames $SR-24-0.75-PHx$ to unveil the impact of the hydrogen fuel lance recess when it is set to $z_i = 4$ mm. For PH20, the flame is intermittently lifted but the mean image shows that it is preferentially stabilised inside the annular injector. For higher hydrogen contents, all flames are aerodynamically stabilised with a flame root lying close to the outlet of the co-axial DFDS burner above the central hydrogen lance. For PH40, the base of the flame has a rounded shape that becomes sharper and more compact in the radial direction for higher hydrogen injection velocities with PH60, PH80 and PH100.

The wider operability range with aerodynamically stabilised flames may again be explained by considering the impulsion ratio J between the two streams. Without recess, it has been shown that flames reattach to the hydrogen nozzle outlet when J takes too small values. In configurations

with a recess of the hydrogen lance, the effective value of J needs to be considered at the DFDS burner outlet corresponding to the location of the combustor backplane and not at the hydrogen lance outlet section, which lies further upstream. Due to the strong internal swirl imparted to the hydrogen stream, the hydrogen jet rapidly expands at the outlet of the central tube at $z_i = 4$ mm in the annular channel leading to a drop of the axial velocity on the centerline at the DFDS burner outlet. The effective impulsion ratio J at the DFDS burner outlet for PH100 reaches thus higher values than $J = 5$ when it is determined at the outlet of the hydrogen lance. This strong radial expansion of the hydrogen stream at the central lance outlet allows injection of high hydrogen flow rates without destabilising the CRZ. This explains the greater range of impulsion ratios J that can be achieved for aerodynamically stabilised flames when the hydrogen lance is inserted inside the burner with a recess.This was also confirmed by tests made for different external injection velocities that are provided as supplemental material. An evaluation of the effective value of the impulsion ratio at the DFDS burner outlet would however require a detailed investigation of the velocity and mixing fields at the DFDS burner outlet, which is out of the scope of the present study.

To summarise, lifted hydrogen enriched flames can be stabilised above a conventional co-axial swirl burner by conferring a strong swirl to the internal hydrogen stream and by slightly shifting the position of the hydrogen lance outlet inside the burner. In agreement with previous observations [19, 20, 21], it is found that without recess and for low values of the momentum ratio J, the flame can reattach to the burner lips when the hydrogen content is increased leading to a drastic reduction of the burner operability with aerodynamically stabilised flames. But experiments also show that a small recess of the hydrogen lance drastically increases the range of operability of the burner with aerodynamically stabilised flames.

3.2. Effect of operating point

In this section, only the geometric configuration SR yielding the widest operability range with aerodynamically stabilised flames is analysed. The influence of equivalence ratio ϕ and bulk velocity u_e on the stabilisation mode and shape taken by the flames is explored for two hydrogen enrichments. The first one is PH40 with methane/air mixture in the external annular channel and

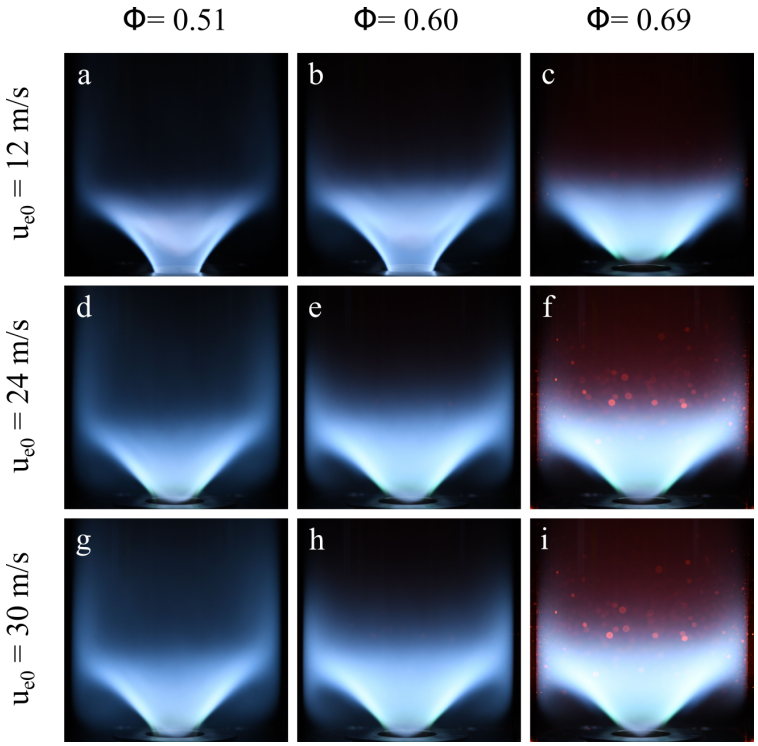

Fig. 5. Effect of the external bulk velocity u_{e0} and equivalence ratio ϕ_0 on flame stabilisation for $SR - u_{e0} - \phi_0 - PH40$. Natural flame emission in the visible spectrum.

pure hydrogen in the central lance. The volumetric ratio of hydrogen in the fuel blend corresponds in this case to $X_{H2} = 0.67$. The second one PH100 is only powered by hydrogen with $X_{H2} = 1.00$ through the central lance and air flowing in the annular channel.

Figure 5 shows nine operating points corresponding to reference bulk velocities $u_{e0} = 12$, 24 and 30 m/s and global equivalence ratio $\phi = 0.51$, 0.60 and 0.69. Flames in Fig. 5a and Fig. 5b are anchored to the central hydrogen lance corresponding to the flame archetype shown in Fig. 2c. In these cases, the hydrogen injection velocity is low $u_i = 5.4$ and 6.4 m/s in Fig. 5a and Fig. 5b respectively compared to the external injection velocity $u_{e0} = 12$ m/s. The CRZ above the central injector is weak. The radial velocity of the swirled hydrogen flow at the central tube outlet is too low to quench the combustion reaction above the injector lip [21]. All other flames in Fig. 5 are lifted and correspond to the flame archetype shown in Fig. 2d due to the higher hydrogen injection velocities, leading to higher radial velocities at the hydrogen lance outlet. The combustion reaction

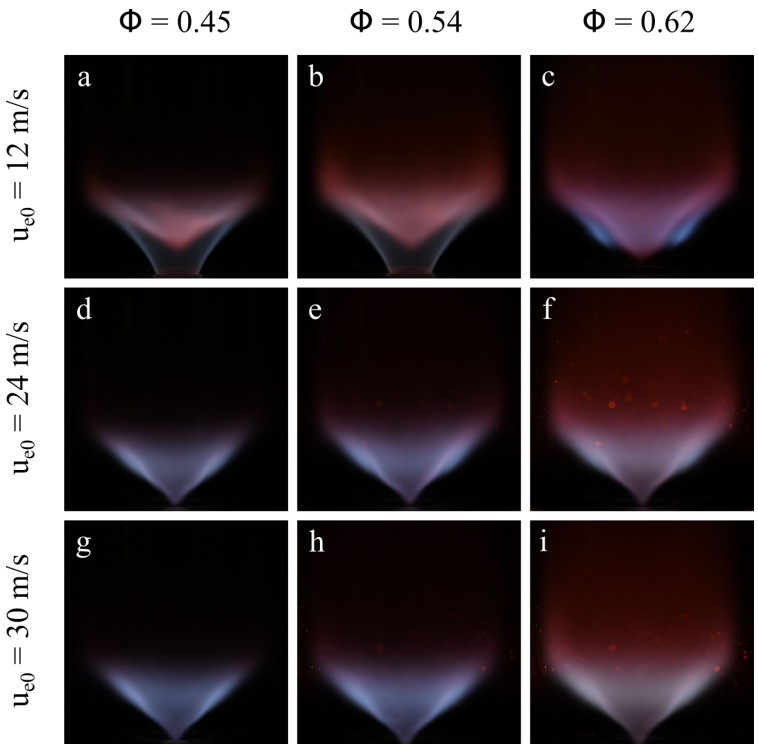

Fig. 6. Effect of the external bulk velocity u_{e0} and equivalence ratio ϕ_0 on flame stabilisation for $SR-u_{e0}-\phi_0-PH100$. Natural flame emission in the visible spectrum.

close to the central tube outlet is submitted to higher radial hydrogen velocities and has more difficulty to take place. An aerodynamic stabilisation mode above the injector becomes more favorable. The lifted flames have a V-shape in Figs. 5c to 5i. Combustion may also take place in the outer recirculation zone when the equivalence ratio or the external bulk velocity increase as in Figs. 5e to 5i. The location of reaction zones is studied in more details in the next section with OH^* images. This figure also shows that for a CH_4/H_2 fuel blend with 40% of power originating from hydrogen, increasing the equivalence ratio at constant external injection velocity (Figs. 5a, b and c) or increasing the hydrogen bulk injection velocity at fixed equivalence ratio (Figs. 5a, d and g) helps lifting the flame.

Figure 6 shows the shape taken by the flames sharing the same reference bulk velocities, reference equivalence ratios and thermal powers as in Fig. 5, but when only hydrogen is used to power the burner. As for PH40, the flames in Figs. 6a and 6b are anchored to the lip of the central hydro-

gen lance and they feature two different reaction branches. The ones stabilised in the shear layer of the swirled flow are sharp with a blue/gray colour attributed to naturally excited $H_2O_2^*$ molecules [27]. The other V-shape structure stabilised in the center of the flow further downstream is orange/red. Schefer and al. [28] attribute this red/orange radiation to H_2O^* chemiluminescence. All other flames in Fig. 6 are aerodynamically stabilised above the burner, but take slightly different shapes compared to Fig. 5. Flames in Fig. 6 are more compact due to the higher reactivity and burning velocity of pure hydrogen compared to the methane/hydrogen blends. The blue luminosity visible in the outer recirculation zone for PH40 in Fig. 5 disappears for PH100 in Fig. 6. The flame root also protrudes further upstream along the burner axis for pure hydrogen with a narrower radial extension. As already observed in Fig. 5 for PH40, increasing the equivalence ratio at constant external injection velocity (Figs. 6a, b and c) or increasing the hydrogen injection velocity at fixed equivalence ratio (Figs. 6a, d and g) helps lifting the flame. The only difference is that the hydrogen lift-off velocity, i.e. the minimum velocity at which hydrogen needs to be injected to obtain a lifted flame increases with the power originating from hydrogen combustion. This is attributed to the higher reactivity of the pure hydrogen flames compared to the hydrogen/methane flames studied in Fig. 5.

This series of experiments highlighting shape transitions also helps understanding the origin of the structure of the reaction layers of the V-shaped aerodynamically stabilised flames powered by pure hydrogen in Fig. 6. When the equivalence ratio is increased from $\phi = 0.45$ to $\phi = 0.62$ and the external annular injection velocity is fixed to $u_{e0} = 12$ m/s, Fig. 6 shows that the orange/red V-shaped structure on the combustion axis progressively protrudes further upstream inside the CRZ at the expense of the blue/gray reaction layers stabilised in the external shear layer of the annular swirled jets that progressively vanishes at the flame bottom. Progressing now along a path at fixed equivalence ratio $\phi = 0.62$ in Fig. 6 and increasing the air velocity to $u_{e0} = 24$ m/s in the annular channel further reduces the reactivity of the external blue reaction layer that is pushed further downstream and completely disappears for $u_{e0} = 30$ m/s. At the same time, the base of the flame progresses further upstream.

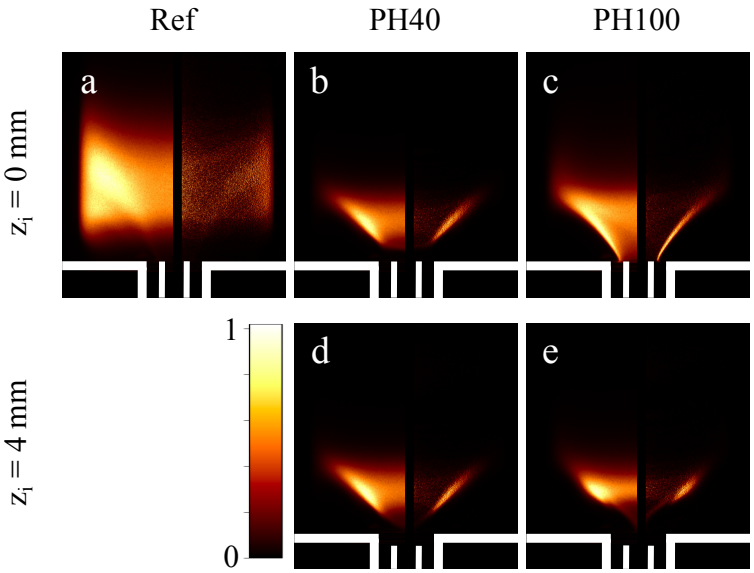

Fig. 7. OH* intensity distribution collected in the line of sight (images on the left) and after Abel deconvolution (images on the right) for $B-24-0.75-PHx$ (top row) and $SR-24-0.75-PHx$ (bottom row).

4. Analysis of the flame structure

To complete direct flame visualisations in the visible band, images restricted to the emission band $\lambda = 310$ nm ± 10 nm centred on the OH* chemiluminescence are now examined. Figure 7 shows the cases $S-24-0.75-PHx$ and $SR-24-0.75-PHx$, where the hydrogen content is varied. The flame in Fig. 7a corresponds to the methane/air fully premixed reference flame when the recess is set to zero, i.e. Ref in the top row in Fig. 4. Flames in Figs. 7b and 7c correspond respectively to $S-24-0.75-PH40$ and $S-24-0.75-PH100$ in the top row in Fig. 4. Flames in Figs. 7d and 7e correspond to $SR-24-0.75-PH40$ and $SR-24-0.75-PH100$ in the bottom row in Fig. 4.

Each image is first normalised by the maximum pixel value of the image. An Abel deconvolution is then applied to get the trace of the signal in the axial plane of the burner [29]. This signal is again normalised by its maximum value.

The Abel deconvoluted images in Fig. 7 can be considered as a rough estimation of the probability of the presence of a reaction layer in the axial plane of the burner. The methane/air premixed reference flame in Fig. 7a features a relatively thick flame brush characterised by strong intermit-

tency leading to a relatively uniform distribution of luminosity in the axial plane of the burner, with a slightly higher probability of presence close to the combustion chamber sidewall. One must keep in mind that the information close to the burner axis is biased due to the rotational symmetry of the Abel inversion. This why information has been masked close to the burner symmetry axis.

When the hydrogen content increases to PH40, the reaction front is better stabilised in the external shear layer of the annular swirling jet due to the higher reactivity of the PH40 fuel blend compared to pure methane and intermittency drastically drops. This is why the flame brush becomes much thinner and more localised in Fig. 7b. When pure hydrogen is injected, the PH100 flame brush becomes sharper in Fig. 7c and extends further upstream and further downstream, again due to the higher reactivity of pure hydrogen compared to a methane/hydrogen blend. This higher reactivity is the reason why the flame can reattach to the central hydrogen lance rim in Fig. 7c without recess $z_i = 0$ mm. Flames in Figs. 7d-e at the bottom show the impact of a $z_i = 4$ mm recess on the flame brush. With recess, the reaction layers in the external shear layers of the burner are pushed further downstream. The impact of the recess is particularly striking for the PH100 flame.

A more detailed analysis would require information on the structure of the velocity field in central recirculation region of the flow, but this is beyond the scope of this study. The next question which is now addressed is the relationship between flame stabilisation and pollutant emissions.

5. Pollutant emissions

Only CO and NOx emissions are considered here. All measurements are normalised by a volumetric fraction of 15% of O_2 in the flue gases. Each value is an average over at least 45 seconds once stationary conditions inside the combustor were met for the selected operating condition. Figure 8 shows the CO (top) and NOx (bottom) concentrations as a function of the fraction of power originating from hydrogen combustion PHx for two internal swirl levels and two recess. The operating point is set to $Geo - 24 - 0.75 - PHx$.

As expected, CO emissions in Fig. 8 drop with the hydrogen content in the fuel blend. There is no clear dependance of CO emissions with the values of the internal swirl level or injector recess distance. CO emisions also do not seem to be correlated to the flame stabilisation mode. A

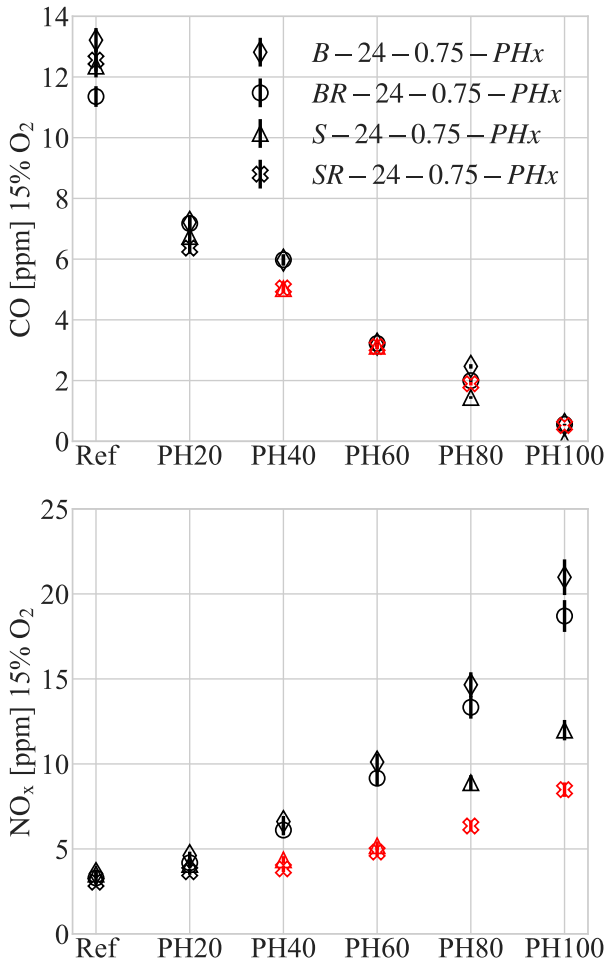

Fig. 8. CO and NOx emissions with error bars as a function of the hydrogen content for different DFDS burner geometries $Geo - 24 - 0.75 - PHx$. Black symbols: Anchored flames. Red symbols: Lifted flames.

residual concentration of CO, less than 1 ppm, is still observed for hydrogen flames, but this level also corresponds to the precision of the CO measurement chain.

NOx measurements are plotted at the bottom in Fig. 8. The lowest detected concentration is approximatively 3 ppm for the fully premixed methane flames. The NOx concentration increases with the hydrogen content injected in the burner. Without inner swirl motion $S_i = 0$, i.e. cases $B - 24 - 0.75 - PHx$ and $BR - 24 - 0.75 - PHx$, NOx emission levels increase rapidly with hydrogen enrichment. For fuel blends with a hydrogen content lower than PH20, NOx emissions are approximatively the same for the different geometrical configurations of the DFDS burner. For

higher hydrogen contents, there is a clear impact of the burner geometry on NOx emissions. They increase much more rapidly when hydrogen is injected without swirl with only a minor effect of the recess.

When the hydrogen stream is swirled with $S_i = 0.9$, i.e. cases $S - 24 - 0.75 - PHx$ and $SR - 24 - 0.75 - PHx$, NOx emissions increase much less with the hydrogen content injected in the burner. In this case, the recess also makes a difference for fuel blends with a hydrogen content higher than PH80. One can link these behaviours to the way the flame is stabilised on the DFDS burner. For PH80 and PH100, the flame reattaches to the central injector rim for the DFDS burner without recess ($S - 24 - 0.75 - PHx$) and remains aerodynamically stabilised with 4 mm recess ($SR - 24 - 0.75 - PHx$). When the flame is anchored to the central hydrogen injection rim, NOx emissions reach higher levels than when the flame is aerodynamically stabilised above the burner. The strong swirl conferred to the hydrogen flow leads to a better mixing with air before combustion. In this latter case, augmenting the recess of the hydrogen lance outlet with respect to DFDS burner outlet further participates to improve mixing of the internal fuel and external oxidiser streams before combustion leading to a reduction by more than 2.5 of NOx emissions with respect to a non swirling hydrogen jet when $S_i = 0$ and $z_i = 0$ mm.

One now further analyses the most promising geometrical configuration explored in this study obtained for the SR geometric configuration. CO and NOx emissions are characterised for $SR - u_{e0} - 0.75 - PHx$ when the hydrogen content is increased for thee different reference bulk velocities $u_{e0} = 12$, 24 and 30 m/s corresponding to different thermal powers $P_{th} = 5.2$, 10.3 and 12.9 kW respectively. As expected, the CO concentration goes to zero with hydrogen enrichment. When the bulk velocity u_{e0} increases CO emissions increase especially for the fully premixed methane/air flames. This is probably due to the quenching of the combustion reaction when the flame impinges the cold flame tube sidewall leading to incomplete combustion. Reducing the bulk velocity u_{e0} by a factor two reduces the CO emissions by a factor three.

The bottom plot in Fig. 9 shows NOx emissions. All flames are aerodynamically stabilised for hydrogen contents exceeding PH40. For the three sets of data, the NOx concentration increases when the hydrogen content increases. However, the observed trend is surprising because NOx emissions decrease when the bulk velocity u_{e0} increases, i.e. when the thermal power increases, at

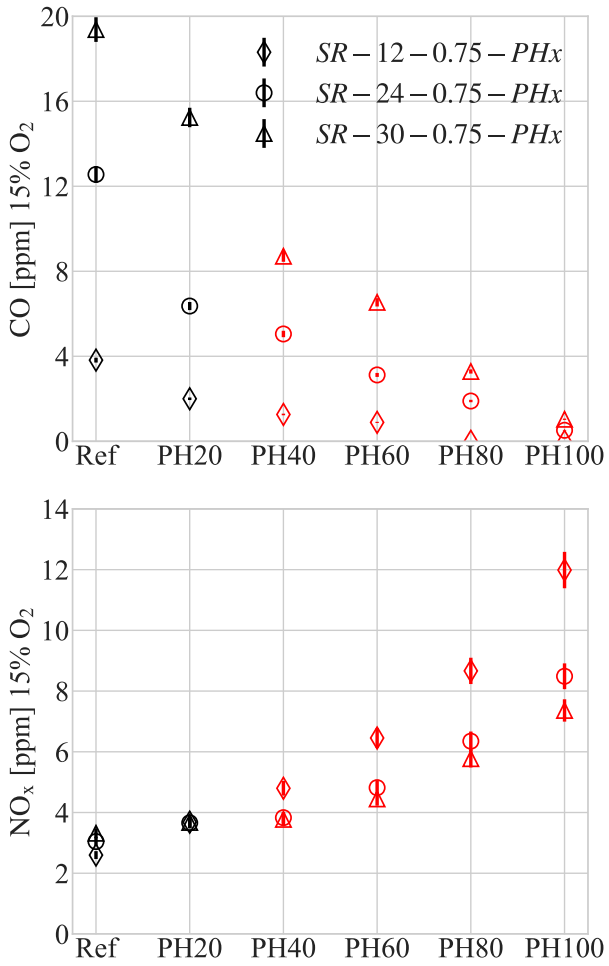

Fig. 9. CO and NOx emissions with error bars as a function of the hydrogen content for $SR - u_{e0} - 0.75 - PHx$. Black symbols: Anchored flames. Red symbols: Lifted flames.

constant reference equivalence ratio $\phi_0 = 0.75$. For the lowest velocity $u_{e0} = 12$ m/s, NOx reaches 12 ppm for the hydrogen air flame and drops to 7 ppm for $u_{e0} = 30$ m/s. This level is particularly low for a hydrogen/air burner operating at $\phi = 0.62$ (see Tab. 1) with a pure hydrogen stream injected 4 mm before the DFDS burner outlet. Industrial burners operate at lower equivalence ratios and secondary air is available to further lower NOx emissions. Moreover, no attempt has been made in this study to optimise the different swirl levels and the recess distance to minimise NOx emissions.

The drop of NOx emissions when increasing the hydrogen injection velocity reveals a better

mixing of air and hydrogen before combustion due to a stronger recirculation of the gases above the coaxial injector. Mixing of the two swirled streams needs to be further investigated by more detailed diagnostics to understand the underlying mechanisms, which is left for further studies.

6. Conclusion

A Dual Fuel Dual Swirl (DFDS) burner operating with methane/air mixtures injected in an annular channel and pure hydrogen injected in a central lance has been presented. Flame stabilisation regimes and pollutant emissions from this burner have been investigated with a series of experiments. Introducing a high swirl in the central hydrogen stream is an efficient way to avoid flame anchoring to the rim of the central lance for hydrogen enriched fuel blends, but is not sufficient to lift the flame for operation with high hydrogen contents. In this latter case, shifting the position of the hydrogen lance with a small recess with respect to the annular channel outlet substantially increases the operability domain of the DFDS burner with lifted flames.

For geometric configurations of the co-axial injector with a small recess and a strong internal swirl, conferring a sufficient injection velocity to the internal hydrogen stream results in lifted flames. Lifted flames stabilise above the DFDS burner in the external shear layers of the annular swirling jet and take a V-shape. For a fixed thermal power, the apex of the V-shaped flame base above the central hydrogen lance narrows and becomes sharper when the hydrogen content injected in the burner increases.

It has been shown that independently of the CH_4/H_2 fuel blend, increasing the equivalence ratio at constant external bulk injection velocity or increasing the hydrogen bulk injection velocity at fixed equivalence ratio helps lifting the flame. The only difference is that the hydrogen lift-off velocity, i.e. the minimum velocity at which hydrogen needs to be injected to obtain a lifted flame increases with the power originating from hydrogen combustion.

At constant thermal power, CO emissions decrease while NOx emissions increase with the hydrogen content injected in the burner. NOx emissions were found to be strongly correlated to the stabilisation mode above the DFDS burner. For a given thermal power, partially premixed flames anchored to the central fuel lance produce large NOx levels that rapidly increase with the hydrogen content. However, emission levels drop by a factor more than 2.5 when the flame is

lifted above the burner indicating a better mixing between the swirled hydrogen stream and the main annular stream before combustion when the flame is lifted. Moreover, for a fixed global equivalence ratio, NOx emissions further reduce when the thermal power increases.

From a technological perspective, the main interesting features of the DFDS burner are:

1. a reduced flashback risk due to the late injection of hydrogen a few millimitres before the combustion chamber
2. a low thermal stress on the solid components of the burner when the hydrogen injection velocity is high enough to lift the flame
3. low NOx emission levels when flames are lifted which are comparable to emissions levels at fully premixed conditions

These observations made in a setup operating at atmospheric conditions for reactants injected at ambient temperature are encouraging. Further work is needed to understand the stabilisation mechanisms and investigate the stabilisation regimes when the inlet temperature and pressure are increased for an adaptation of the DFDS burner to conventional gas turbine combustors.

Acknowledgments

This project has received funding from the European Research Council under the European Union's Horizon 2020 research and innovation programme Grant Agreement 832248, SCIROCCO and under the Horizon 2020, COEC (Center of Excellence in Combustion) program, Grant Agreement 952181.

References

[1] P. Chiesa, G. Lozza, L. Mazzocchi, Using hydrogen as gas turbine fuel, Journal of Engineering for Gas Turbines and Power 127 (1) (2005) 73–80. doi:10.1115/1.1787513.

[2] K.-K. Lam, P. Geipel, J. Larfeldt, Hydrogen enriched combustion testing of siemens industrial sgt-400 at atmspheric conditions, Journal of Engineering for Gas Turbines and Power 137 (2) (2015) 021502 (7 pages).

[3] M. Bothien, A. Ciani, J. Wood, G. Fruechtel, Toward decarbonized power generation with gas turbines by using sequential combustion for burning hydrogen, Journal of Engineering for Gas Turbines and Power 141 (12) (2019) 121013 (10 pages).

[4] O. Tuncer, S. Acharya, J. Uhm, Dynamics, nox and flashback characteristics of confined premixed hydrogen-enriched methane flames, International Journal of Hydrogen Energy 34 (1) (2009) 496–506. doi:10.1016/j.ijhydene.2008.09.075.

[5] S. Taamallah, K. Vogiatzaki, F. Alzahrani, E. Mokheimer, M. Habib, A. Ghoniem, Fuel flexibility, stability and emissions in premixed hydrogen-rich gas turbine combustion : Technology, fundamentals, and numerical simulations, Applied Energy 154 (2015) 1020–1047. doi:10.1016/j.apenergy.2015.04.044.

[6] G. Richards, M. McMillian, R. Gemmen, W. Rogers, S. Cully, Issues for low-emission, fuel-flexible power systems, Process in Energy and Combustion Science 27 (2) (2001) 141–169. doi:10.1016/S0360-1285(00)00019-8.

[7] T. Reichel, C. Paschereit, Interaction mechanisms of fuel momentum with flashback limits in lean-premixed combustion of hydrogen, International Journal of Hydrogen Energy 42 (2017) 4518–4259.

[8] G. Dahl, F. Suttrop, Engine control and low-nox combustion for hydrogen fuelled aircraft gas turbines, International Journal of Hydrogen Energy 23 (8) (1998) 695–704.

[9] F. Cozzi, A. Coghe, Behavior of hydrogen-enriched non-premixed swirled natural gas flames, International Journal of Hydrogen Energy 31 (6) (2006) 669–677.

[10] J. Oh, J. Hwang, Y. Yoon, Einox scaling in a non-premixed turbulent hydrogen jet with swirled coaxial air, International Journal of Hydrogen Energy 16 (2010) 8715–8722.

[11] H. H.-W. Funke, N. Beckman, J. Keinz, A. Horikawa, 30 years of dry low nox micromix combustor research for hydrogen-rich fuels : an overview of past and present activities, Journal of Engineering for Gas Turbines and Power 143 (7) (2021) 071002 (13 pages).

[12] N. Syred, J. Beér, Combustion in swirling flows: A review, Combustion and Flame 23 (1974) 143–201.

[13] T. Reichel, K. Goeckeler, O. Paschereit, Investigation of lean premixed swirl-stabilized hydrogen burner with axial air injection using oh-plif imaging, Journal of Engineering for Gas Turbines and Power 137 (11) (2015) 1–10. doi:10.1115/1.4031181.

[14] S. Joo, S. Kwak, Y. Yoon, Effect of h2 enrichment ratio and n2/co2 dilution on swirl-stabilized partially premixed h2/ch4/c3h8 sng combustion, International Journal of Hydrogen Energy 45 (2020) 31255–31267.

[15] T. Dixon, J. Truelove, T. Wall, Aerodynamic studies on swirled coaxial jets from nozzles with divergent quarls, Journal of Fluids Engineering 105 (2) (1983) 197–203. doi:10.1115/1.3240964.

[16] M. Durbin, M. Vangsness, D. Bailal, V. Katta, Study of flame stability in a step swirl combustor, Journal of Engineering for Gas Turbines and Power 118 (2) (1996) 308–315. doi:10.1115/1.2816592.

[17] R.-H. Chen, J. Driscoll, J. Kelly, M. Namazian, W. Schefer, A comparison of bluff-body and swirl-stabilized flames, Combustion Science and Technology 71 (4-6) (1990) 197–217.

[18] S. Chouaieb, W. Kriaa, H. Mhiri, P. Bournot, Swirl generator effect on a confined coaxial jet characteristics, International Journal of Hydrogen Energy 42 (2017) 29014–29025.

[19] S. Yuasa, Effect of swirl on the stability of jet diffusion flames, Combustion and Flame 66 (2) (1986) 181–192.

[20] A. Degeneve, C. Mirat, J. Caudal, R. Vicquelin, T. Schuller, Effects of swirl on the stabilization of non-premiexed oxygen-enriched flames above coaxial injectors, Journal of Engineering for Gas Turbines and Power 141 (12) (2019) 121018 (9 pages). doi:10.1115/1.4045024.

[21] A. Degeneve, R. Vicquelin, C. Mirat, J. Caudal, T. Schuller, Impact of co- and counter-swirl on flow recirculation and liftoff of non-premixed oxy-flames above coaxial injectors, Proceedings of the Combustion Institute 38 (4) (2021) 5501–5508. doi:10.1016/j.proci.2020.06.279.

[22] G. Oztarlik, L. Selle, T. Poinsot, T. Schuller, Suppression of instabilities of swirled premixed flames with minimal secondary hydrogen injection, Combustion and Flame 214 (2020) 266–276.

[23] D. Laera, P. Agostinelli, L. Selle, Q. Cazères, G. Oztarlik, T. Schuller, L. Gicquel, T. Poinsot, Stabilization mechanisms of ch4 premixed swirled flame enriched with a non-premixed hydrogen injection, Proceedings of the Combustion Institute 38 (4) (2021) 6355–6363. doi:10.1016/j.proci.2020.06.378.

[24] S. Richard, C. Viguier, S. Marragou, T. Schuller, Dispositif d'injection de dihydrogène et d'air (FR Patent No FR2111267), Institut National de la Propriété Industrielle, 2021.

[25] R. Price, I. Hurle, T. Sugden, Optical studies of the generation of noise in turbulent flames, Symposium (International) on Combustion 12 (1) (1969) 1093–1102. doi:10.1016/S0082-0784(69)80487-X.

[26] T. Mahmud, J. Truelove, T. Wall, Flow characteristics of swirling coaxial jets from divergeant nozzles, Journal of Fluids Engineering 109 (3) (1987) 275–282. doi:10.1115/1.3242661.

[27] T. Fiala, T. Sattelmayer, Heat release and uv-vis radiation in non premixed hydrogen-oxygen flames, Experiments in Fluids 56 (7) (2015) 1–15.

[28] R. W. Schefer, W. D. Kulatilaka, B. D. Patterson, T. B. Settersten, Visible emission of hydrogen flames, Combustion and Flame 156 (6) (2009) 1234–1241.

[29] S. N. Simons, Z.-G. Yuan, The filtered abel transform and its application in combustion diagnostics, NASA Technical Report Server, NASA/CR—2003-212121.

Supplementary material

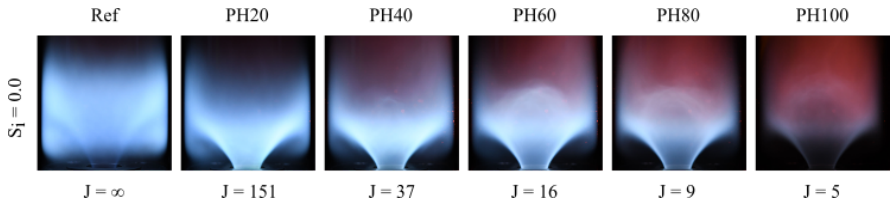

Fig. 1. Effect of the injector recess on flame stabilisation for $BR - 24 - 0.75 - PHx$. Images are recorded in the visible spectrum.

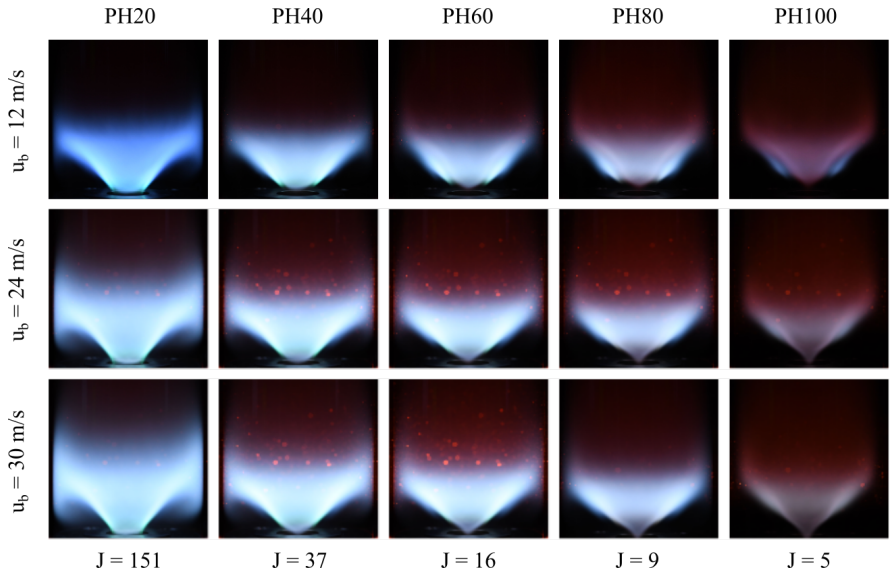

Fig. 2. Effect of air bul velocity on flame stabilisation for $SR - u_{e0} - 0.75 - PHx$. Images are recorded in the visible spectrum.